

Continuous two-wave lasing in microchip Nd:YAG lasers

I.E. Ievlev, I.V. Koryukin, Yu.S. Lebedeva, P.A. Khandokhin

Abstract. Simultaneous two-wave lasing was obtained in microchip end-pumped Nd:YAG lasers at the wavelengths of 1061.5 and 1064.17 nm at room temperature. Laser wave intensities were studied as functions of crystal temperature and pump power. The ranges of parameters were determined in which the two-wave lasing occurs and the reasons for such lasing were established. A model is suggested, which adequately describes the experimental results obtained.

Keywords: Nd:YAG laser, two-wave lasing, gain profile, level structure, transition cross section.

1. Introduction

The interest in studying simultaneous lasing at several wavelengths in a laser [1–8] is explained by a possible employment of such regimes in some applications as resonance holographic interferometry, optical communications, environment monitoring, laser radars, generation of terahertz radiation. The main lasing transitions in Nd³⁺ ions, which have relatively high emission cross sections, are those between the multiplets $^4F_{3/2} \rightarrow ^4I_{11/2}$ and $^4F_{3/2} \rightarrow ^4I_{13/2}$. The transitions with the wavelengths $\lambda = 1064.15$ and 1338.1 nm are most frequently used in developing Nd:YAG lasers. In some experiments, simultaneous lasing at 1064 and 1318 nm was observed [1–3]. These transitions have the common upper working level (level A in Fig. 1a, the transition corresponding to $\lambda = 1318$ nm is not shown). Since the transition cross section at 1064 nm is several times greater than that at 1318 nm simultaneous lasing at both transitions is only possible if special efforts are made to reduce the cavity Q factor at the wavelength of 1064 nm.

In the vicinity of $\lambda = 1064$ nm, there is one more transition with a high emission cross section at 1061.5 nm. As was shown in [9–11], the cross section of this transition depends noticeably on the crystal temperature: at low temperatures it dominates. In cooling the laser crystal to a temperature $T \sim 230$ K, the lasing thresholds at 1064 and 1061.5 nm became close and simultaneous lasing at these two wavelengths was observed. However, at room temperatures, no emission was observed at $\lambda = 1061.5$ nm in the lasers generating many longitudinal modes.

I.E. Ievlev, I.V. Koryukin, Yu.S. Lebedeva, P.A. Khandokhin
Institute of Applied Physics, Russian Academy of Sciences,
ul. Ul'yanova 46, 603950, Nizhnii Novgorod, Russia;
e-mail: khando@appl.sci-nnov.ru

Received 19 January 2011; revision received 14 June 2011
Kvantovaya Elektronika 41 (8) 715–721 (2011)
Translated by N.A. Raspopov

The present work is devoted to investigation of the continuous lasing in a microchip Nd:YAG lasers at $\lambda = 1061.5$ and 1064.17 nm. To our knowledge, this is a first report on simultaneous lasing at the mentioned wavelengths at a room temperature. In what follows, we will call the simultaneous lasing at the wavelengths centred at $\lambda = 1061.5$ and 1064.17 nm the two-wave lasing regime irrespectively of the number of the longitudinal modes generated in a particular line.

Note that in addition to possible practical applications of such lasers there is an interest in revealing the reasons that impede two-wave lasing. In our point of view, the common upper level contributing into the gains at these two wavelengths is the key factor, to which the present work is devoted.

2. Experimental setup

Microchip lasers under study are the plane-parallel plates made of yttrium aluminum garnet doped with neodymium, with a diameter of ~ 10 mm and various thicknesses (cavity lengths). Dielectric mirrors forming the cavity are deposited onto the plane faces of the plates. In addition, the input faces have antireflection coatings at the pump wavelength of 810 nm and output faces have reflecting coatings at the same wavelength. The concentration of active ions Nd³⁺ in the crystals is 1 at. %.

The structure of laser transitions at the wavelengths $\lambda = 1064.17$ and 1061.5 nm is presented in Fig. 1a [12, 13]. The line at 1064.17 nm is formed by two transitions at the wavelengths $\lambda = 1064.15$ nm with the cross section $\sigma_1 = 7.1 \times 10^{-19}$ cm² (at $T = 300$ K) and $\lambda = 1064.4$ nm with $\sigma_2 = 1.9 \times 10^{-19}$ cm² [13]. This structure of the line mainly determines the dynamics of a ring Nd:YAG laser [14]. The weak transition (at $\lambda = 1064.4$ nm) has the common upper lasing level B with the transition at 1061.5 nm ($\sigma_3 = 4.7 \times 10^{-19}$ cm²), which should hinder obtaining simultaneous lasing at 1064.17 and 1061.5 nm. In Fig. 1b, the gain profiles for yttrium aluminum garnet with neodymium are shown for the transitions presented in Fig. 1a. At $T = 300$ K, the line widths at $\lambda = 1064.17$ and 1061.5 nm are close and equal to 190 GHz [13].

A schematic diagram of the experimental setup is shown in Fig. 2. Linearly polarised radiation of a laser diode was focused by a system of lenses L1 and L2 to a surface of the active element (microchip laser). A filter F at the output of the Nd:YAG laser was used to cut off the pump radiation from a detection channel. A heating element controlled the crystal temperature, measured by an electronic thermometer. The radiation was detected by an optical spectroanalyser with the resolution of 0.05 nm. Mutual adjustment of the pump and microchip-laser beams provided generation of a fundamental transversal mode TEM₀₀. In the experiments, four microchip Nd:YAG lasers were used with the thicknesses $L = 0.5, 1, 2,$

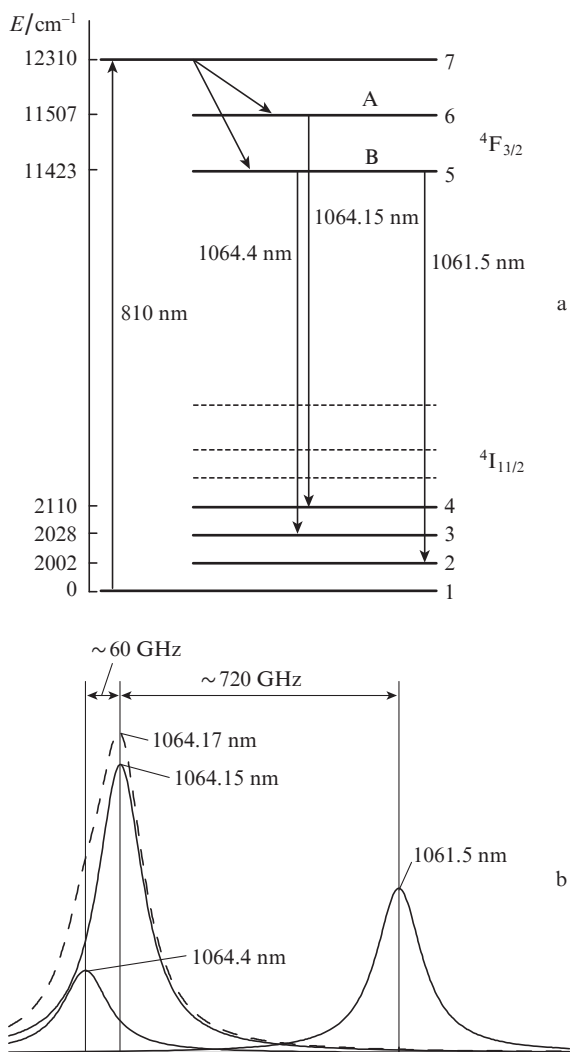


Figure 1. Structure of laser transitions in ions Nd^{3+} in yttrium aluminum garnet (a) and the corresponding gain profiles (b).

and 4 mm. At such cavity lengths, the gain profiles of each transition comprised from one (for $L = 0.5$ mm) to four–five longitudinal modes.

3. Experimental results

In the experiments, the power of lasing modes was studied as a function of two parameters – the crystal temperature and pump power. It is worth noting that the variation in the active element temperature from 25°C to 90°C weakly affected the transition cross section (and the linear gain of an active medium) at 1061.5 nm, in contrast to [9], where the range of temperature variation was much wider. Hence, in our experiments, the main effect of temperature variation is the change in the optical cavity length, which affects the frequencies of longitudinal modes, i.e., scanning of the cavity modes through the gain profiles of the active medium. Estimates show that heating of an active element changes a longitudinal mode frequency by the value $\delta\nu = -3 \text{ GHz K}^{-1}$ due to mutual action of thermo-optical and thermal expansion effects. The change in the mode spacing was in this case insufficient (less by three orders of magnitude).

Two-wave lasing was observed in all the samples. Figure 3 shows a typical optical spectrum of two-wave lasing for the sample with the cavity length of 0.5 mm. Dependences of the mode power on the crystal temperature for the cavity length of 0.5 mm are presented in Fig. 4. In this laser, two-wave lasing occurs over the whole range of temperature variation. One can clearly see the effect of mode frequency tuning versus temperature: in the fundamental line ($\lambda = 1064.17$ nm) one mode ceases at $T \sim 50^\circ\text{C}$ as the detuning from the line centre becomes sufficiently large, whereas the other mode approaching the line centre starts generation at $T \sim 68^\circ\text{C}$. Here, the central mode emits over the whole range of temperature variation and has a maximum at $T \sim 60^\circ\text{C}$. With increasing the cavity length, the range of two-wave lasing converges. This effect is demonstrated in Fig. 5, where the threshold pump powers for generating the strong and weak lines are shown versus the crystal temperature at various cavity lengths. Thus, in a laser with the 4 -mm-long cavity, the two-wave lasing only occurs at a high pump power in a narrow range of temperature variation ($\Delta T \approx 10^\circ\text{C}$).

Obviously, optimal conditions for two-wave lasing occur at the mode spacing comparable to the gain widths and providing single-mode lasing in each of the transitions. Just such a case was realised in our experiments with the shortest chip laser (Fig. 5,a): the spacing between neighbouring longitudinal modes $\Delta\nu$ was ~ 165 GHz, which is comparable with the gain profile width at the spacing between the lines $\Delta\nu_{12} = 720$ GHz ($\Delta\nu_{12} - 4\Delta\nu = 60$ GHz). Thus, by varying the crystal tempera-

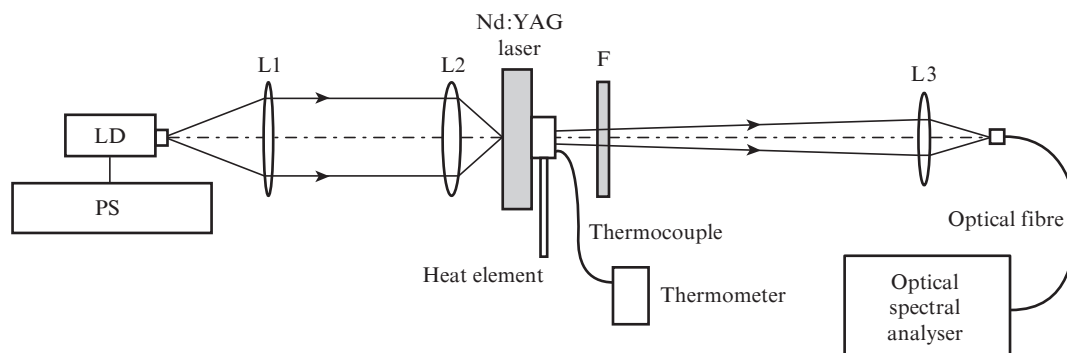


Figure 2. Schematic diagram of the experimental setup: (PS) power supply of the pump laser; (LD) pump laser diode ($\lambda = 810$ nm); (L1, L2, L3) collecting lenses; (F) spectral filter at $\lambda = 810$ nm.

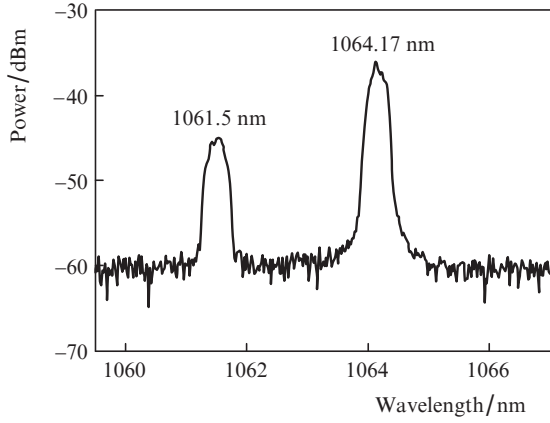


Figure 3. Optical spectrum of a laser with a 0.5-mm-long cavity at the pump power $P = 1$ W.

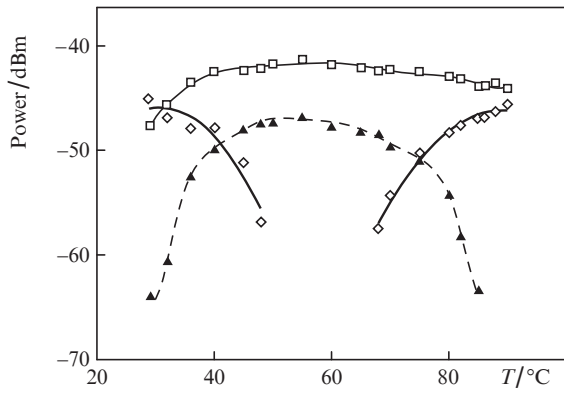


Figure 4. Mode power vs. laser crystal temperature at $L = 0.5$ mm, $P = 1$ W. Solid curves correspond to the strong mode (\square) and two weak modes (\diamond) for the line at $\lambda = 1064.17$ nm. The dashed curve is the radiation power at $\lambda = 1061.5$ nm.

ture and tuning the longitudinal mode comb relative to the gain profiles we provided conditions needed for two-wave lasing. By transferring to longer samples (Figs 5c, d) we reduce the mode spacing, which results in generation of several longitudinal modes at the line with $\lambda = 1064.17$ nm and in a higher saturation of its weak component (1064.4 nm). This causes a reduction of the gain for the line $\lambda = 1061.5$ nm and, correspondingly, increases the threshold pump power at this wavelength.

4. Results of theoretical considerations

The considerations given above were taken into account in developing a model of a multimode Nd:YAG laser. The model is based on the well-known Tang–Statz–DeMars system of equations [15, 16]. The equations were generalised to the case of a three-line gain assuming that each cavity mode interacts with all the lines. In addition, the allowance was made for relaxation transitions between the closely residing upper levels A and B of the term ${}^4F_{3/2}$. Finally, we obtain the following system of equations

$$\begin{aligned} \frac{dI_k}{d\tau} &= GI_k [g_k^{(1)}(D_0 - D_k) + (g_k^{(2)} + g_k^{(3)})(N_0 - N_k) - 1], \\ \frac{dD_0}{d\tau} &= A - D_0 \left(1 + \sum_{m=1}^M g_m^{(1)} I_m \right) + \sum_{m=1}^M g_m^{(1)} I_m D_m \\ &\quad - w_{AB} D_0 + w_{BA} N_0, \\ \frac{dD_k}{d\tau} &= - \left(1 + \sum_{m=1}^M g_m^{(1)} I_m \right) D_k + \frac{1}{2} g_k^{(1)} I_k D_0 \\ &\quad - w_{AB} D_k + w_{BA} N_k, \end{aligned} \quad (1)$$

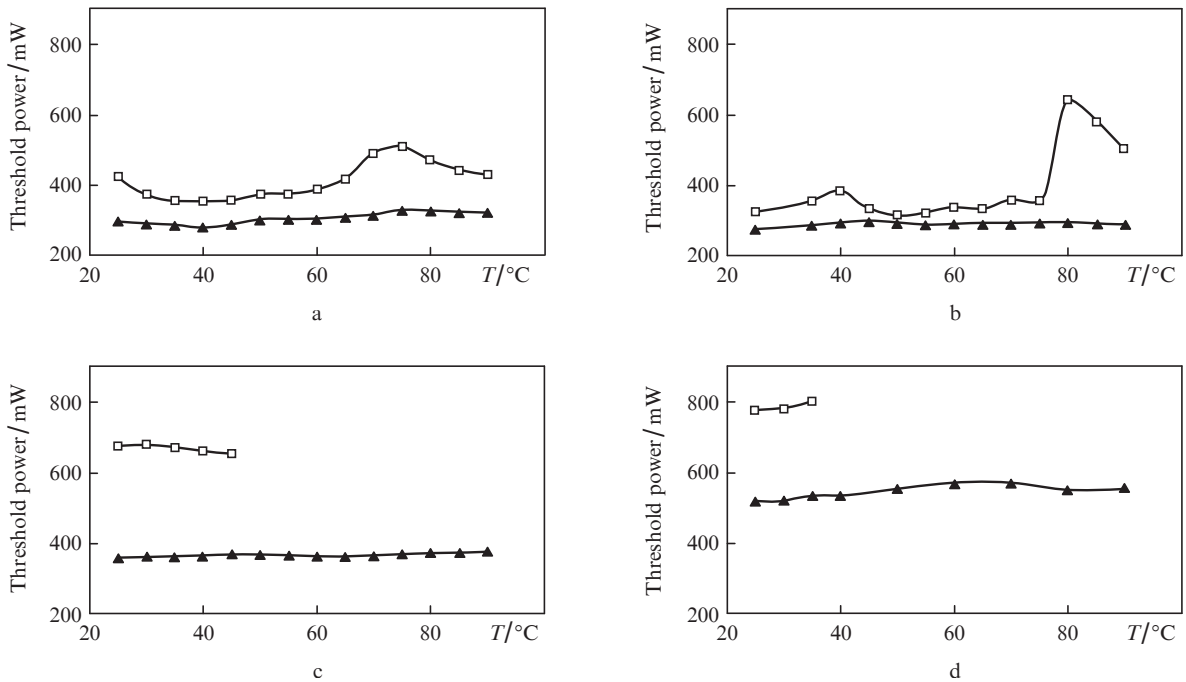


Figure 5. Threshold pump power for lasing at 1061.5 nm (\square) and 1064.17 nm (\blacktriangle) vs. crystal temperature for the laser cavity lengths $L = 0.5$ (a), 1 (b), 2 (c), and 4 mm (d).

$$\begin{aligned}\frac{dN_0}{d\tau} &= A - N_0 \left[1 + \sum_{m=1}^M (g_m^{(2)} + g_m^{(3)}) I_m \right] \\ &\quad + \sum_{m=1}^M (g_m^{(2)} + g_m^{(3)}) I_m N_m - w_{BA} N_0 + w_{AB} D_0, \\ \frac{dN_k}{d\tau} &= - \left[1 + \sum_{m=1}^M (g_m^{(2)} + g_m^{(3)}) I_m \right] N_k \\ &\quad + \frac{1}{2} (g_k^{(2)} + g_k^{(3)}) I_k N_0 - w_{BA} N_k + w_{AB} D_k.\end{aligned}$$

Here, I_k are the intensities of lasing modes normalised to the saturation intensity of the transition $6 \rightarrow 4$ ($\lambda = 1064.15$ nm); A is the pump parameter; D_0 and D_k are the spatially homogeneous inversion and the population inversion gratings, respectively, for the transition with the upper lasing level A; N_0 and N_k are the spatially homogeneous inversion and the corresponding inversion gratings for the transition with the upper lasing level B; w_{BA} and $w_{AB} = w_{BA}/w$ are the rates of relaxation transitions between levels A and B;

$$w = \exp\left(\frac{E_B - E_A}{k_B T}\right); \quad (2)$$

E_A and E_B are the energies of levels A and B, respectively; k_B is the Boltzmann constant [16]; M is the number of longitudinal modes; $G = 2\kappa/\gamma_{\parallel}$; $\tau = t\gamma_{\parallel}$; γ_{\parallel} and κ are the relaxation rates for the population inversion and for the field in a cavity, respectively. Equations (1) take into account all the three lines mentioned with the gains (see Fig. 1b)

$$\begin{aligned}g_k^{(1)} &= L_k^{(1)}, \quad g_k^{(2)} = \frac{\sigma_2}{\sigma_1} L_k^{(2)}, \quad g_k^{(3)} = \frac{\sigma_3}{\sigma_1} L_k^{(3)}, \\ L_k^{(1)} &= \{1 + [(p-k)\Delta_0 - \Delta]^2\}^{-1}, \\ L_k^{(2)} &= \{1 + [(p-k)\Delta_0 - \Delta - \Delta_2]^2\}^{-1}, \\ L_k^{(3)} &= \{1 + [(p-k)\Delta_0 - \Delta + \Delta_3]^2\}^{-1}, \\ \Delta_2 &= \frac{\omega_0^{(2)} - \omega_0^{(1)}}{\gamma_{\perp}} \approx -0.7, \quad \Delta_3 = \frac{\omega_0^{(3)} - \omega_0^{(1)}}{\gamma_{\perp}} \approx 9, \\ \Delta_0 &= \frac{\omega_{k+1} - \omega_k}{\gamma_{\perp}}, \quad \Delta = \frac{\omega_0^{(1)} - \omega_p}{\gamma_{\perp}},\end{aligned} \quad (3)$$

where γ_{\perp} is the half-width of the homogeneous gain profile (for the considered transitions, γ_{\perp} is equal to $\sim 80-90$ GHz); Δ_0 is the mode spacing; $\omega_0^{(1)}$ is the gain profile centre for the transition $\lambda = 1064.15$ nm; ω_p is the frequency of the nearest to the gain centre mode with an index p ; Δ is the detuning of this mode from the centre of the gain profile; $\omega_0^{(2)}$ and $\omega_0^{(3)}$ are the centres of the gain profiles at $\lambda = 1064.4$ and 1061.5 nm, respectively. A variation of the detuning Δ leads to a shift of the longitudinal mode comb relative to all the three gain profiles.

Origin of the two-wave lasing and its specific features in the case of the shortest laser cavity may be explained in the framework of a simplified model. First, we neglect the weak component of the line at 1064.17 nm by assuming $g_k^{(2)} = 0$. Using the experimental results we may limit our consideration to one mode generated in the line with $\lambda = 1061.5$ nm

and neglect the population inversion grating N_k burnt by the mode. We also assume that each mode interacts with only one gain line. In this case, the system of equations (1) becomes substantially simpler and takes the form

$$\begin{aligned}\frac{dI_k}{d\tau} &= GI_k [g_k^{(1)} (D_0 - D_k) - 1], \\ \frac{dI_{\alpha}}{d\tau} &= GI_{\alpha} [g_{\alpha}^{(3)} N_0 - 1], \\ \frac{dD_0}{d\tau} &= A - D_0 \left(1 + \sum_{m=1}^M g_m^{(1)} I_m \right) + \sum_{m=1}^M g_m^{(1)} I_m D_m \\ &\quad - w_{AB} D_0 + w_{BA} N_0, \\ \frac{dD_k}{d\tau} &= - \left(1 + \sum_{m=1}^M g_m^{(1)} I_m \right) D_k + \frac{1}{2} g_k^{(1)} I_k D_0, \\ \frac{dN_0}{d\tau} &= A - N_0 (1 + g_{\alpha}^{(3)} I_{\alpha}) - w_{BA} N_0 + w_{AB} D_0,\end{aligned} \quad (5)$$

where α is the index of the only mode generated in the line with $\lambda = 1061.5$ nm.

A stationary solution to system (5) can be found analytically for an arbitrary number of modes M , generated in the gain band with $\lambda = 1064.15$ nm:

$$\begin{aligned}I_k &= \frac{D_0 - 1/g_k^{(1)}}{g_k^{(1)} [S_1 - (M - 0.5)D_0]}, \quad I_{\alpha} = A - \frac{1 + w_{BA}}{g_{\alpha}^{(3)}} + w_{AB} D_0, \\ D_k &= D_0 - \frac{1}{g_k^{(1)}}, \quad N_0 = \frac{1}{g_{\alpha}^{(3)}}, \\ D_0 &= \frac{A}{2} + \frac{2S_1 + w_{AB} - \sqrt{R}}{2M - 1}, \\ R &= [2S_1 + A(M - 0.5) + w_{AB}]^2 \\ &\quad - 4(M - 0.5)(AS_1 + S_2 + w_{BA}/g_{\alpha}^{(3)}), \\ S_1 &= \sum_{m=1}^M \frac{1}{g_m^{(1)}}, \quad S_2 = \sum_{m=1}^M \left(\frac{1}{g_m^{(1)}} \right)^2.\end{aligned} \quad (6)$$

This is a generalisation of the stationary solution for the Tang–Statz–DeMars system of equations obtained in [17] to the considered case of two gain lines. The dependences of stationary mode intensities versus the detuning Δ (the crystal temperature) calculated for a 0.5-mm-long laser cavity are shown in Fig. 6. One can see that the dependences well agree qualitatively with the experiment (see Fig. 4). The lasing at 1064.15 nm comprises at most two modes, which also agrees with the experiment (see Fig. 3). In the calculation, the relaxation rates $w_{BA} = 0.2$ and $w_{AB} = w_{BA}/w = 0.3$ ($w \approx 0.67$ at room temperature) were used, which provide the best correspondence with the experimental data. Study of an influence of these parameters on intensities of lasing modes has shown that their reduction causes an increase in the intensity of the mode generated in the weak gain line (1061.5 nm). Thus, simple model (5) adequately describes the experimental results for a short-cavity laser (with a large mode spacing). A reduction of the mode spacing and, consequently, increase in the num-

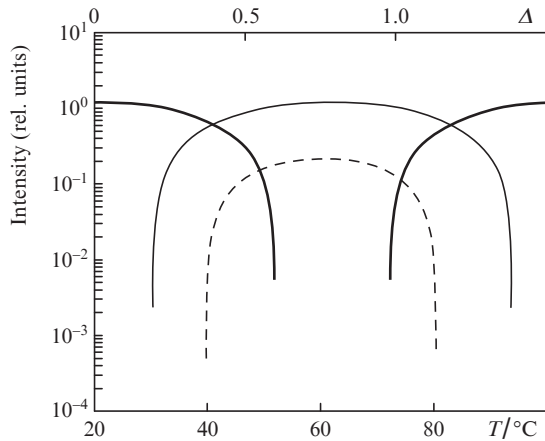
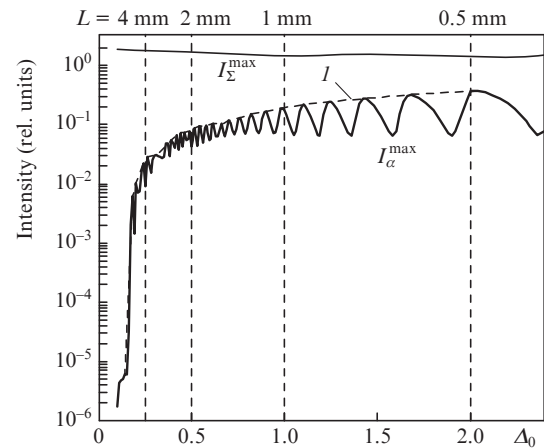


Figure 6. Mode intensities vs. detuning Δ (the crystal temperature) for the laser with a 0.5-mm-long cavity; stationary solution (6) of simplified model (5) at $A = 2$, $w_{BA} = 0.2$, and the rate of mode detuning -3 GHz K^{-1} . Solid curves correspond to the intensities of modes generated at 1064.17 nm, the dashed curve corresponds to mode intensities at 1061.5 nm.

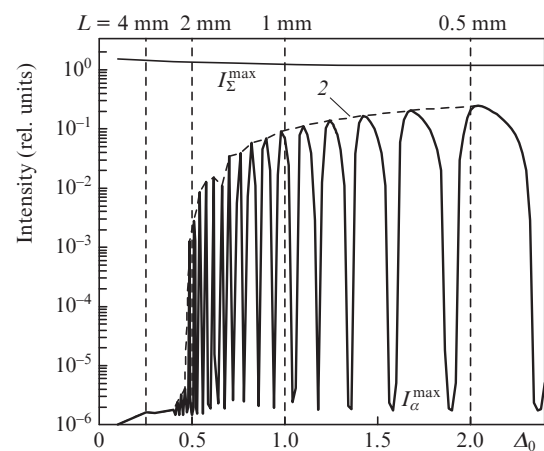
ber of modes in the strong line lead to a decrease in the intensity of the mode in the weak line; however, this mode is not totally suppressed. This confirms our assumption that a description of the experimental results obtained with longer laser cavities should take into account a contribution of the weak line at $\lambda = 1064.4 \text{ nm}$.

It is impossible to find a stationary solution for the complete system of equations (1) analytically. Hence, it was found by integrating numerically system (1). In the calculations, all parameters were fixed except for the detuning Δ , whose variations modelled a variation in the crystal temperature. At different mode spacings Δ (lengths of a chip laser), the dependences similar to those given in Fig. 6 were calculated, from which the maximal intensity I_{α}^{\max} for the mode generated on the transition $5 \rightarrow 2$ ($\lambda = 1061.5 \text{ nm}$) and the maximum total intensity I_{Σ}^{\max} of all the longitudinal modes generated in the strong line ($\lambda = 1064.17 \text{ nm}$) were found. The resulting dependences $I_{\alpha}^{\max}(\Delta_0)$ and $I_{\Sigma}^{\max}(\Delta_0)$ are presented in Fig. 7 at two values of the pump parameter A . One can see that the dependences $I_{\alpha}^{\max}(\Delta_0)$ are not monotonic and demonstrate high sensitivity of the lasing conditions in the weak line to positions of cavity mode frequencies relative to the centre of active medium gain profile. Nevertheless, a common tendency is observed for a reduction of the mode intensity in the weak line [curves (1) and (2) drawn through the maxima of $I_{\alpha}^{\max}(\Delta_0)$] at smaller mode spacings and, consequently, for an increase in the number of modes generated in the strong line (from one-two at $\Delta_0 = 2$ to six-seven at $\Delta_0 = 2$). This confirms the above assertion that the multimode lasing in the strong transition is the reason of suppressing lasing in the weak transition.

Data from Fig. 7 were obtained not taking into account relaxation processes between the upper lasing levels ($w_{BA} = w_{AB} = 0$). In using simple model (5), it was shown that the relaxation exchange between these levels plays an important role in establishing lasing at various wavelengths. In the experiment, the temperature of the active element varied from 20°C to 80°C , which, according to (2), should affect the relaxation rates. Dependences of the maximal radiation intensity in the weak line with these parameters taken into account are shown in Fig. 8 versus the mode spacing. For comparison, curve (1) from Fig. 7a is also given in the figure. One can see



a



b

Figure 7. I_{α}^{\max} and I_{Σ}^{\max} vs. mode spacing Δ_0 at the pump parameter $A = 2.0$ (a) and 2.2 (b), $w_{BA} = w_{AB} = 0$. Curves (1) and (2) are plotted through maxima of $I_{\alpha}^{\max}(\Delta_0)$. Vertical lines mark the cavity lengths corresponding to Δ_0 .

that at a large mode spacing comparable with the width of a gain profile, the relaxation processes between the upper lasing levels result in an increase in the radiation intensity at 1061.5 nm. An opposite situation is observed at small mode spacings, where lasing in the strong line includes a great number of longitudinal modes. In addition to the tendency mentioned above, Fig. 8 demonstrates a reduction of the radiation intensity generated in the weak line at a higher crystal temperature [compare curves (1') and (1'')]. It is shown that the reduction of the radiation intensity at 1061.5 nm is related to a higher lasing threshold for this transition.

Figure 9 shows the dependence of the threshold pumping parameter for the weak line on the mode spacing for the parameters corresponding to curves (1') and (1'') from Fig. 8. One can see that a change in the relaxation rate ratio w in raising the crystal temperature results in an increase in the lasing threshold. This effect is revealed in the dependence of the radiation intensity in the weak line on the detuning Δ (crystal temperature) at various cavity lengths, which is clearly demonstrated in Fig. 10. In calculating such dependences in the system of equations (1), synchronously with a variation of the parameter Δ the parameter w also varies from 0.67 at $T = 20^{\circ}\text{C}$ ($\Delta = 0$) to 0.78 at $T = 80^{\circ}\text{C}$ ($\Delta = 2$). One can see that at a large mode spacing ($\Delta_0 = 2$), account for the temperature

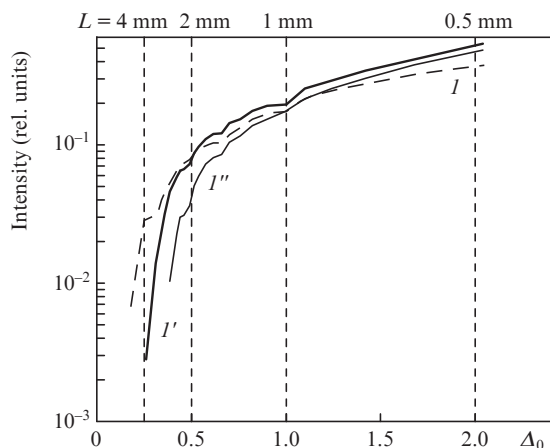


Figure 8. Intensity I_{α}^{\max} vs. mode spacing Δ_0 at $T = 20^{\circ}\text{C}$, $w_{\text{BA}} = 0.2$, $w_{\text{AB}} = w_{\text{BA}}/w = 0.3$, $w = 0.67$ (I'); $T = 80^{\circ}\text{C}$, $w_{\text{BA}} = 0.2$, $w_{\text{AB}} = 0.256$, $w = 0.78$ (I'') at a fixed pump parameter $A = 2.0$. For comparison, curve (I) from Fig. 7a is shown.

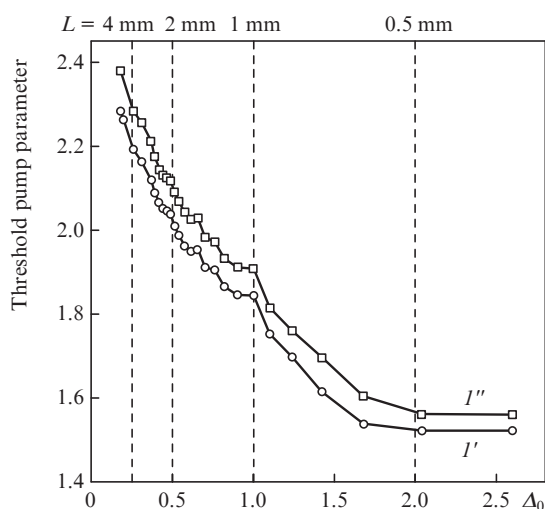


Figure 9. Threshold pump parameter for the weak line as a function of mode spacing under conditions that correspond to curves (I') and (I'') in Fig. 8.

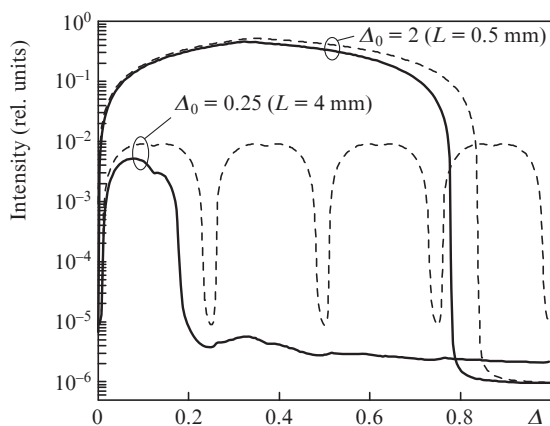


Figure 10. Radiation intensity for the weak line vs. longitudinal mode detuning frequency Δ at synchronous variation in relaxation parameters w_{BA} and w_{AB} for two limiting values of the mode spacing (solid curves). Dashed curves are calculated at fixed parameters $w_{\text{BA}} = 0.2$ and $w_{\text{AB}} = 0.3$ ($w = 0.67$).

dependence of parameters w_{AB} and w_{BA} weakly affects the intensity behaviour of the weak line. A completely different situation occurs at the small mode spacing ($\Delta_0 = 0.25$): comparatively small variations in the parameter Δ (small variations in the crystal temperature) suppress lasing in the weak transition, which well agrees with the experimental data presented in Fig. 5.

5. Conclusions

Continuous two-wave mode lasing at 1061.5 and 1064.17 nm was found and investigated in monolithic microchip Nd:YAG lasers with various cavity lengths at room temperature. The optical length of the active element was varied by heating, which provided tuning the longitudinal mode frequencies relative to the centres of the gain lines. Thus, we varied the laser frequency within homogeneous widths of each of the gain lines. Two-wave lasing was observed in all samples under investigation; however, the range of parameters, in which such lasing occurs, became substantially narrower at longer cavities. The two-wave lasing in a narrow sense, i.e., the generation of a single frequency (a longitudinal mode) in each of the two gain profiles only occurred in the laser with the shortest cavity 0.5 mm in length. In lasers with longer cavities, usually several longitudinal modes were generated in the transition at $\lambda = 1064.17$ nm.

A reduction of the mode spacing by transferring to longer samples (Figs 5c, d) leads to generation of several longitudinal modes in the line at 1064.17 nm and to a greater saturation of its weak component (1064.4 nm). Consequently, the gain at 1061.5 nm decreases and, correspondingly, the lasing threshold at this wavelength increases.

A model is proposed, which includes the three transitions in ions Nd^{3+} contributing into the gain at the wavelengths under study. The model makes allowance for relaxation transitions between close upper laser levels (the levels A and B of the term $^4\text{F}_{3/2}$). It is shown that at a longer cavity and greater number of the modes generated within the gain profile at 1064.17 nm, the weak component of the latter (at 1064.4 nm) is more saturated. Hence, the gain at 1061.5 nm reduces and, correspondingly, the lasing threshold at this wavelength increases, thus narrowing the pump range, in which the generation of the weak line was observed. The range of temperatures, in which the two-wave lasing occurred, also became narrower. This effect was also explained in the framework of the suggested model.

The experimental and theoretical investigations show that the simultaneous lasing at the wavelengths 1061.5 and 1064.17 nm at room temperature requires that single-mode lasing on the strong transition at 1064.17 nm was provided. This is only possible in lasers with a short cavity of at most 0.5 mm long. One more possibility is to use lasers with a ring cavity, where only single-mode lasing is realised [18–21].

Acknowledgements. The work was supported by the Program of the RF President for State Support of Leading Scientific Schools (Grant No. NSh-3800.2010.2).

References

1. Bethea C.G. *IEEE. J. Quantum Electron.*, **9**, 254 (1973).
2. Kalintsev A.G., Khazov L.D. *Zh. Prikl. Spektrosk.*, **24** (6), 1073 (1976) [*J. Appl. Spectrosc.*, **24**, 765 (1976)].

3. Nadtocheev V.E., Nanii O.E. *Kvantovaya Elektron.*, **16**, 680 (1989) [*Sov. J. Quantum Electron.*, **19**, 444 (1989)].
4. Shen H.Y., Zeng R.R., Zhou Y.P., Yu G.F., Huang C.H., Zeng Z.D., Zhang W.J., Ye Q.J. *IEEE J. Quantum Electron.*, **27**, 2315 (1991).
5. Zhou R., Wen W., Cai Z., Ding X., Wang P., Yao J. *Chin. Opt. Lett.*, **3**, 597 (2005).
6. Saha A., Ray A., Mukhopadhyay S., Sinha N., Datta P.K., Dutta P.K., *Opt. Express*, **14**, 4721 (2006).
7. Lunstedt K., Pavel N., Petermann K., Huber G. *Appl. Phys. B*, **86**, 65 (2007).
8. Wu B., Jiang P., Yang D., Chen T., Kong J., Shen Y. *Opt. Express*, **17**, 6004 (2009).
9. Kushida T., *Phys. Rev.*, **185**, 500 (1969).
10. Birnbaum M., Klein C.F. *J. Appl. Phys.*, **44**, 2928 (1973).
11. Brauch U. *Appl. Phys. B*, **58**, 397 (1994).
12. Kushida T., Marcos H.M., Geusic J.E. *Phys. Rev.*, **167**, 289 (1968).
13. Zverev G.M., Golyaev Yu.D. *Lazery na kristallakh i ikh primeneniye* (Crystal Lasers and Their Applications) (Moscow: Radio i svyaz', 1994) p. 38.
14. Koryukin I.V., Khandokhin P.A., Khanin Ya.I. *Opt. Commun.*, **81**, 297 (1991).
15. Tang C.L., Statz H., DeMars G. *J. Appl. Phys.*, **34**, 2289 (1963).
16. Khanin Ya. I. *Principles of Laser Dynamics* (Amsterdam, North-Holland: Elsevier, 1995; Moscow: Nauka, 1999).
17. Pieroux D., Mandel P. *Opt. Commun.*, **107**, 245 (1994).
18. Khandokhin P.A., Khanin Ya.I. *J. Opt. Soc. Am. B*, **2**, 226 (1985).
19. Kravtsov N.V., Lariontsev E.G. *Kvantovaya Elektron.*, **27**, 98 (1999) [*Quantum Electron.*, **29**, 378 (1999)].
20. Gelikonov V.M., Stepanov D.P., Khandokhin P.A., Turkin A.A., Mamaev Yu.A., Shirokov E.Yu. *Proc. SPIE Int. Soc. Opt. Eng.*, **2792**, 74 (1996).
21. Mamaev Yu.A., Milovskii N.D., Turkin A.A., Khandokhin P.A., Shirokov E.Yu. *Kvantovaya Elektron.*, **27**, 228 (1999) [*Quantum Electron.*, **29**, 505 (1999)].